Preparation and Mechanical Properties of High-Performance Short Ramie Fiber-Reinforced Polypropylene Composites

Yulin Feng, Yuexin Hu, Guiyan Zhao, Jinghua Yin, Wei Jiang

State Key Laboratory of Polymer Physics and Chemistry, Changchun Institute of Applied Chemistry, Chinese Academy of Sciences, Changchun 130022, People's Republic of China

Received 16 August 2010; accepted 31 January 2011
DOI 10.1002/app.34281
Published online 26 May 2011 in Wiley Online Library (wileyonlinelibrary.com).

ABSTRACT: Short ramie fiber (RF) was used to reinforce the polypropylene (PP). The composites were prepared in a twin-screw extruder followed by injection molding. The experimental results showed that both the strength and the modulus of the composites increase considerably with increasing RF content. The tensile strength and flexural strength are as high as 67 and 80 MPa by the incorporation of ramie up to 30 wt %. To the best of our knowledge, this is one of the best results for short natural fiber-reinforced PP composites. However, the preparation method in this study is more simple and economic. This short RF-reinforced PP composites extend the application field for short-nature fiber-reinforced PP composites. Morphological analysis revealed that it is the high aspect ratio of the fiber and good interfacial compatibility that result in the high performance of the composites. © 2011 Wiley Periodicals, Inc. J Appl Polym Sci 122: 1564–1571, 2011

Key words: biofibers; polypropylene; reinforcement; composites; mechanical properties

INTRODUCTION

The use of natural fibers as reinforcement for composites in place of glass and other synthetic fibers has received increasing attention from both research and industrial communities for many years.[1–6] The prospective benefits of the natural fiber reinforced composites are derived from the properties of the natural fibers such as renewability, biodegradability, low cost, low density, acceptable specific mechanical properties, ease of separation, and carbon dioxide sequestration.[7–9]

The combination of the bast fibers of annual fiber crops like flax,[10,11] hemp,[12,13] sisal,[2,9] jute,[14–16] kenaf,[17] or ramie with the relatively cheap polypropylene (PP) yields material with an interesting price/performance ratio, which can be used as, for instance, interior parts in cars. However, the problem of poor compatibility between the polar hydrophilic natural fiber and the nonpolar hydrophobic PP results in difficulties in compounding of these materials and poor stress-transfer efficiencies.[13] Enhanced interfacial adhesion for composites containing natural fiber can be achieved either by fiber and matrix modification with chemical/physical treatments or by the use of interfacial additives. Of all these attempts, maleic anhydride-grafted PP (PP-*g*-MAH) has been extensively used as compatibilizers in various polyolefin composites with natural fibers.[18,19]

Ramie, commonly known as China grass, is widely planted in both southern and northern china. Several researchers have exploited the reinforcing potential of ramie fibers (RFs) for developing thermoplastic and thermoset composites using different processing techniques. Ramie in the form of nonwoven fiber mat was used as reinforcement for thermoset resins such as soy protein-based resin[20,21] and for thermoplastics such as PLA.[22] In these studies, the processing of the composites was mainly by compressing molding and the *in situ* polymerization method. Few studies have been done on the use of chopped or short RFs as reinforcement by melt processing with thermoplastics matrix followed by injection molding, which is a more simple and economic method than press molding method.

In this study, we tried to prepare the PP composites with high strength by using short RFs as reinforcement. The purpose of this work is to give a

Correspondence to: G. Zhao (gyzh@ciac.jl.cn) or W. Jiang (wjiang@ciac.jl.cn).

Contract grant sponsor: Major Program; contract grant number: 50833005.
Contract grant sponsor: Funds for Distinguished Young Investigators; contract grant number: 50725312.
Contract grant sponsor: National Natural Science Foundation of China (Creative Research Groups); contract grant number: 50921062.
Contract grant sponsor: Jilin Province (Research Program); contract grant number: 20080506.

TABLE I
Formulation of Composites

Designation of samples	PP (wt %)	Rime fiber (wt %)	Compatibilizer (wt %)
1	87	10	3
2	77	20	3
3	67	30	3
4	70	30	0

facile and economic preparation and give a new insight into the relation between structure and properties for high-performance natural fiber-reinforced PP composites.

EXPERIMENTAL

Materials

PP (Moplen EP 501L, melt flow index = 6 g/10 min with a load of 2.16 kg at 230°C) was obtained from Basell. Maleic anhydride-grafted PP (Fusabond® MD353D) was obtained from DuPont Company. Short RF used in the study was obtained from Chengdu Wanhe Chemical Company with average fiber length of 6 mm, width of 10 μm, tensile strength of 628 MPa, modulus of 74 GPa, elongation of 3.6%, and the crystallinity of 64%.

Sample preparation

The short RF was dried in a vacuum oven at 80°C for 24 h before processing. Extrusions with various fiber loading were carried out in a Haake Polylab System (RC500P) with twin-screw extruder at the temperature range of 160–200°C and 80 rpm. PP or a mixture of PP and MAPP was fed upstream; the fibers were fed downstream in the molten polymer. The pellets from extrusion were used to obtain specimens for mechanical properties by injection molding. Formulation of the composites prepared for this study is given in Table I.

Mechanical measurements

The tensile and flexural properties were measured on an Instron universal testing instrument (INSTRON112) at the loading rate of 10 mm/min at room temperature. The Notched Izod impact test was carried out with a XJU-22 impact tester (Chengde Test Machine Company, China) at room temperature. Five specimens of each composition were tested, and average values were reported.

Dynamic mechanical analysis (DMA) of the rectangular specimens with dimensions of 4.0 × 9.0 × 1.0 mm was conducted on DMA/SDTA861^e (Mettler Toledo, Switzerland) in the tensile mode. The samples were scanned from −50 to 180°C at a frequency of 1 Hz and a heating rate of 3°C/min. The storage modulus E' and loss factor (tan δ) were recorded as a function of temperature.

Fiber length distribution

The fibers were separated from the PP matrix by extraction with xylene, and then the fibers were laid on a microscope glass slide and observed with an Olympus BX51 Microscope (Olympus, Tokyo, Japan). Fiber length was measured by direct measurement of the micrographs with ImageJ software. Hundred fibers for each sample were analyzed and recorded.

Morphological observation

The fracture surfaces from the tensile tests and the morphology of RF before processing were examined using a scanning electron microscopy (SEM) at room temperature. A JEOL (model JXA-2010) SEM with field emission gun and accelerating voltage of 100 keV was used to collect SEM images for the specimens. All specimen surfaces were sputter coated with a thin layer of gold (~20 nm) before examination.

Small-angle X-ray scattering

Small-angle X-ray scattering (SAXS) experiments were performed using a NanoSTAR-U (BRUKER AXS) with Cu Kα radiation. The generator was operated at 40 kV and 650 mA. Two-dimensional SAXS patterns were obtained using a HI-STAR detector. The sample-to-detector distance was L_{SD} = 1074 mm. The effective scattering vector q at this distance range from 0.05 to 2 nm^{-1}.

Wide angle X-ray diffraction

Wide angle X-ray diffraction (WAXD) was performed on a Rigaku D/MAX 2500 V PC X-ray diffractometer (Japan) in reflection mode using the monochromated Cu Kα radiation from a Riguku generator operated at 40 kV and 200 mA. An angle range of 5°–40° was scanned at 4°/min for every sample.

Differential scanning calorimetry

The thermal behavior of the blends was investigated using differential scanning calorimetry (DSC) with a TA DSC-2920 instrument. All samples were heated to 200°C and held for 3 min to eliminate the influence of thermal history. A scanning rate of 10°C min^{-1} was adopted. The weight of the samples was about 5–10 mg. All measurements were performed under nitrogen atmosphere.

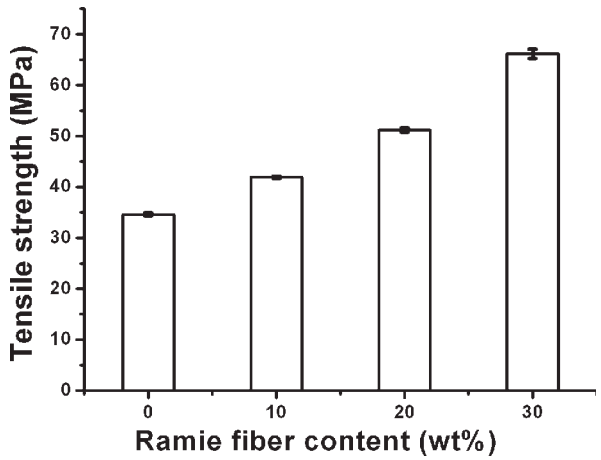

Figure 1 Effect of ramie fiber content on the tensile strength of the composites.

The degree of crystallinity (X_c) of the PP/RF composites can be determined from their heat of fusion normalized to that of the PP according to the following equation:

$$X_c = \frac{\Delta H_m}{\Delta H^*} \times 100\%$$

where $\triangle H_m$ is the melting heat of the PP/RF composite normalized to that of PP and $\triangle H^*$ is the melting heat of PP with 100% crystallinity, and the values of $\triangle H^*$ is 240.5 J/g.[23]

RESULTS AND DISCUSSION

Mechanical properties

The tensile strength of short RF-reinforced PP composites is shown in Figure 1 as a function of the RF loading. The results indicate that the tensile strength increases with increasing ramie content, for the composite containing 30 wt % RF, the tensile strength is as high as 67 MPa, which is 97% higher than that of pure PP. Although many researches have been done in the field of bast fiber-reinforced PP composites by injection molding, few studies presented such high tensile strength as reported in this study. Panthapulakkal and coworkers[12] found that the value of 58 MPa for tensile strength was achieved from a hybrid composite containing 25 wt % of hemp and 15 wt % of glass. Bledzki et al.[23] used abaca fibers and man-made cellulose to reinforce PP and found that the values of tensile strength were up to 44 and 72 MPa, respectively, for the composites containing 30 wt % abaca fiber or man-made cellulose. Although the tensile strength of man-made cellulose-reinforced PP composites is relatively higher than that reported in this work, man-made cellulose fibers are produced in chemical–technical viscose processes, and the cost is relatively high compared to bast fibers such as ramie, hemp, sisal, jute, and flax fibers. So, the natural fiber-reinforced PP composites with high mechanical strength can be fabricated with relatively cheap RF compared to man-made cellulose.

In general, the tensile strength of short fiber-reinforced composites mainly depends on fiber volume, fiber aspect ratio, fiber–matrix adhesion, and fiber orientation. The high tensile strength in this research might be due to (1) the high aspect ratio of the RF distributed in the PP matrix, which will be confirmed by measurement of RF length under light microscopy and (2) the good adhesion between the fibers and PP by adding MAPP coupling agent, and so the stress can be transferred effectively from the matrix to the stronger fibers, which will be confirmed by SEM observation. More details will be discussed in the last two sections.

The reinforcement effect of short RF on the tensile modulus of PP/RF composites is shown in Figure 2. It is seen that the tensile modulus of ramie fiber-reinforced PP composite increases considerably with an increase in the RF content.

Flexural strength reflects the ability of the material to withstand bending forces applied perpendicular to its longitudinal axis. Flexural strength of the composites is plotted in Figure 3 as a function of the ramie content. It is shown that the flexural strength of the composite increased linearly with increasing RF content, for the composite containing 30 wt % RF, the flexural strength is as high as 80 MPa, which is 74% higher than that of pure PP.

The flexural modulus of the PP/RF composites increases significantly compared to pure PP as the RF content increases (Fig. 4). For the composite containing 30 wt % RF, the flexural modulus is 80% higher than that of the unreinforced polymeric matrix.

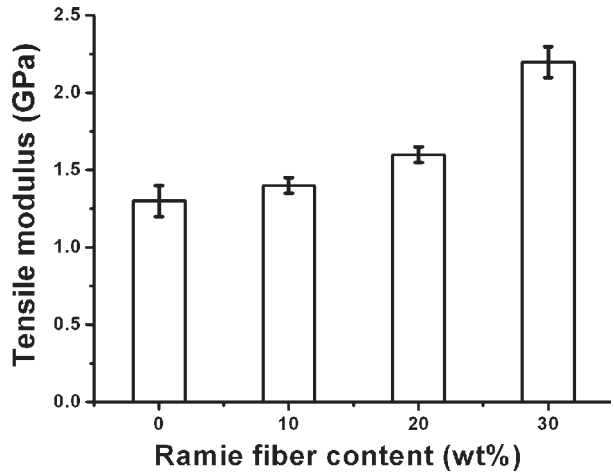

Figure 2 Effect of ramie fiber content on the tensile modulus of the composites.

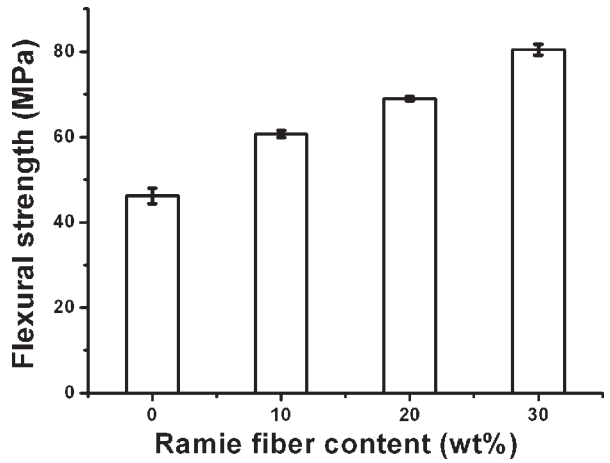

Figure 3 Effect of ramie fiber content on the flexural strength of the composites.

The impact strength of composites reflects the ability of the material to resist the fracture failure under stress applied at high speed and is directly related to the toughness of the material. The fibers play an important role in the impact resistance of fiber-reinforced composites as they interact with the crack formation and act as stress-transferring medium. Variation of notch Izod impact strength of PP/RF composites with RF content is shown in Figure 5. The results indicate that the impact strength increases slightly from 2.8 to 4.7 kJ/m^2 with the RF content increasing from 0 to 30 wt %. The enhancement of toughness is due to the suppression of fiber/matrix debonding and fiber pull-out as a result of the compatibilization effect of the MAPP-coupling agent. Xie et al.[24] studied the composites of PP/sisal fiber and obtained a similar result.

Figure 6 shows the variation of the storage modulus with the temperature detected from DMA test for the PP/RF blends with various RF contents. For

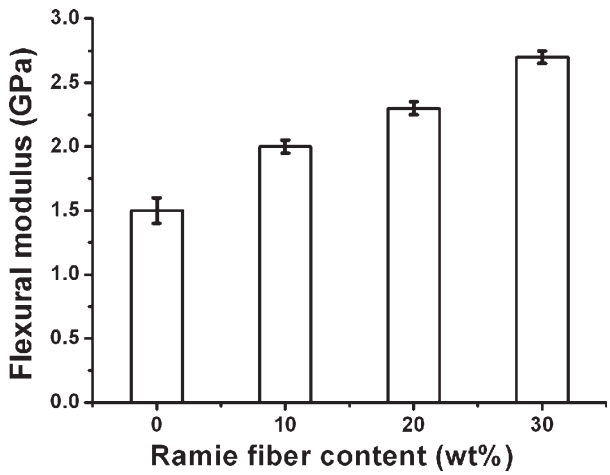

Figure 4 Effect of ramie fiber content on the flexural modulus of the composites.

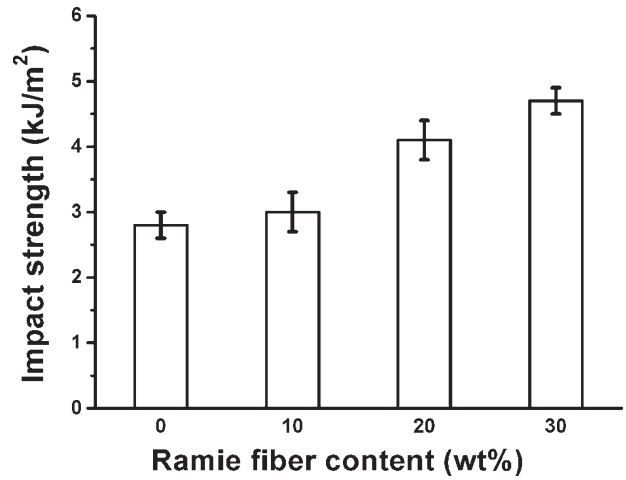

Figure 5 Effect of ramie fiber content on the notched Izod impact strength of the composites.

a given stress or modulus level, the higher temperature corresponds to a higher temperature resistance. To evaluate the heat resistance of the composites, we define the temperature at $E' = 1.0$ GPa as $T_{E'=1.0}$. From Figure 6, it is known that $T_{E'=1.0}$ is 44°C for pure PP and $T_{E'=1.0}$ is 112°C for the blend containing 30 wt % RF. These results reveal that the heat-deflection temperature of PP can be much improved by the incorporation of RF.

Figure 7 shows that β (glass) transition peak shifts to a lower temperature as the amount of RF loading increases. Sanadi et al.[25] suggested that the incorporation of natural fiber and improvement of interfacial adhesion could lead to the increase of the transition temperature by restricting the mobility of polymer chains. This indicates that they cannot lead to the lowing of the transition temperature. On the other hand, the presence of low molecular weight of

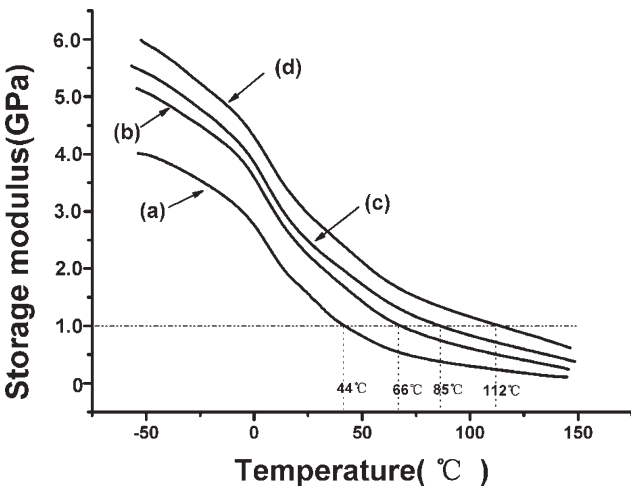

Figure 6 Temperature dependence of the storage modulus of the composites (a) neat PP, (b) PP/MAPP/RF (87/3/10), (c) PP/MAPP/RF (77/3/20), and (d) PP/MAPP/RF (67/3/30).

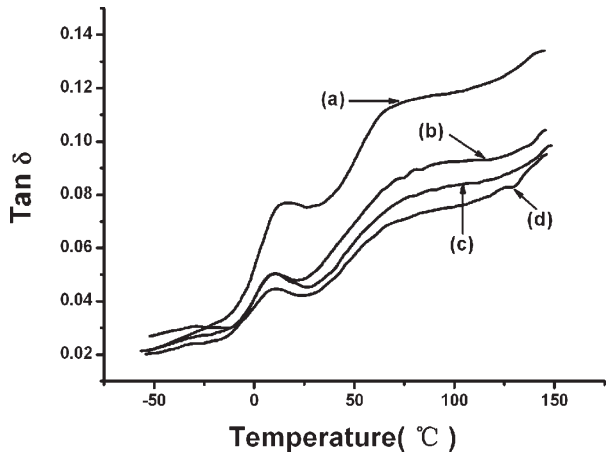

Figure 7 Temperature dependence of the tan δ of the composites (a) neat PP, (b) PP/MAPP/RF (87/3/10), (c) PP/MAPP/RF (77/3/20), and (d) PP/MAPP/RF (67/3/30).

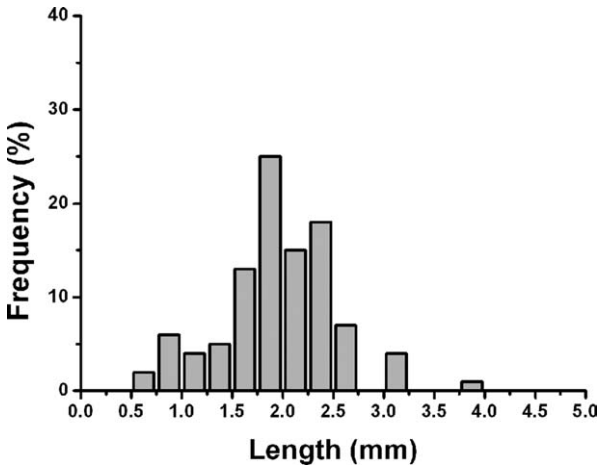

Figure 8 Distribution of fiber lengths of composite with 30 wt % ramie fiber and 3 wt % MAPP after extrusion followed by injection molding.

MAPP and sheared surface material from the natural fibers during the melting processing could reduce the transition temperature by enhancing the mobility of polymer chains.[26] In this study, the amount of coupling agent MAPP remains unchanged for all composites. This means that the content for residual MAPP should be lower for higher fiber content. As a result, the transition temperature should increase with increasing the fiber content. However, this contradicts with the experimental result in Figure 7. Therefore, it is the sheared materials including lignin, cellulose, oils, and other surface extractives that result in the decrease of the transition temperature with increasing fiber content. This can be further supported by the evidence that the composite with higher fiber content is easier to get dark after injection molding.

The α transition is related to the relaxation of restricted PP amorphous chains in the crystalline phase (defects).[25,26] From Figure 7, it can be seen that the intensity of α transition increases with the addition of the RF. It is thus inferred that the presence of large amount RFs restricts the mobility of the PP chains in the crystalline zone and causes more defects in the crystalline phase.

Distribution of fiber lengths

Fiber breakages take place during the processing of short fiber composites. The reduction of fiber length is caused mainly by (1) fiber–fiber interaction (2); fiber interaction with polymer matrix (3); fiber contact with equipment surfaces. Eventually, there exists a fiber length distribution in injection-molded short fiber-reinforced thermoplastics.[27] Figure 8 shows the fiber length distribution of RF extracted from injection-molded sample of 30 wt % fiber loading. The extracted RF exhibits a narrow fiber length distribution with more than 70% of fibers are distributed in the rage of 1.50–2.50 mm. The average fiber length of RF before compounding is 6.0 mm. It is reduced to 2.0 mm after processing, which is much higher than the data reported in literatures.[10,12,15] In general, the average fiber length remaining after

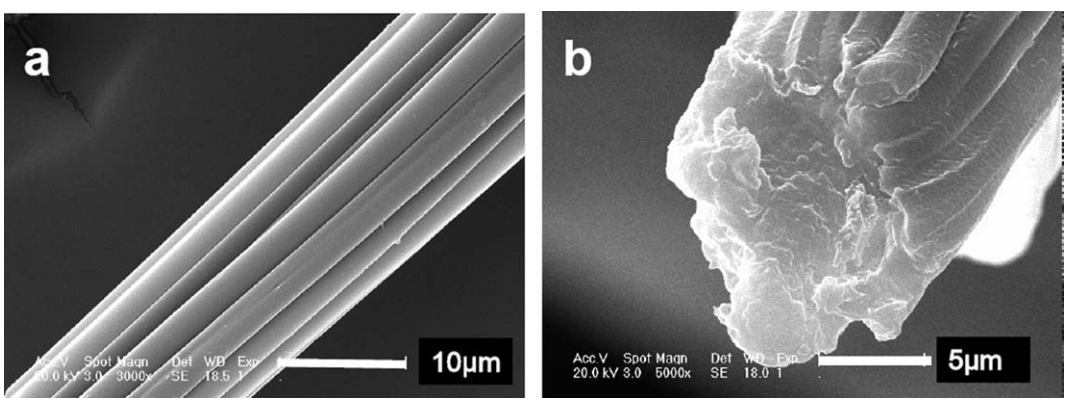

Figure 9 SEM micrographs of ramie fiber before processing (a) longitudinal section and (b) cross section.

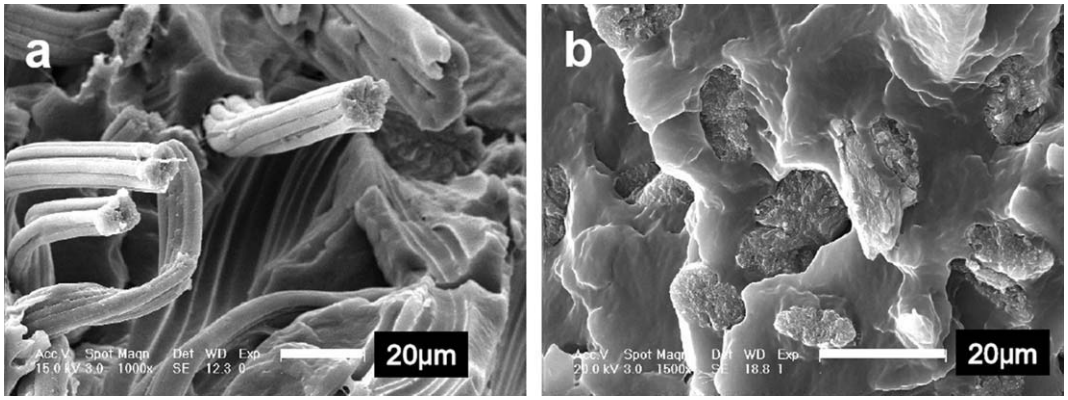

Figure 10 Fractured surfaces of compounds of 30 wt % ramie fiber/PP (a) without MAPP and (b) with 3 wt % MAPP.

processing is one of the most important factors determining the ultimate mechanical properties of the composites. So, the high tensile strength in this study can mainly be attributed to the long fibers distributed in the matrix.

Morphology

Figure 9 shows SEM micrographs of the longitudinal and cross section of the fiber before compounding with PP. The cross section of fiber in Figure 9(b) shows that the diameter of the fiber is about 10 μm, while after injection, the diameter of the fiber remains almost unchangeable as shown in Figure 10(a). So, the fibers exhibit the length and diameter of 2.0 mm and 10 μm, respectively, after extrusion followed by injection molding. The result shows that the fibers possess high L/D ratio (about 200). That is one of the main reasons that lead to the high tensile strength of the composites.

Figure 10 shows SEM micrographs of tensile fracture surfaces of samples with 30 wt % RF content. For the PP/RF composite without MAPP [Fig. 10(a)], most fibers are pulled out from the matrix. Moreover, their surface are quite smooth, indicating the adhesion between matrix and fibers is weak. However, for the PP/RF composite with MAPP [Fig. 10(b)], most fibers are fully embedded within the PP matrix, indicating that the adhesion between PP and RF is strong.

Crystallization and thermal properties

To study the relation between the PP lamella thickness and the tensile strength of the composites, pure PP and the PP/RF composites were investigated using SAXS. According to the methodology proposed by Glatter,[28] the plots of Iq^2 versus q is shown in Figure 11. It is seen that the position of maximum scattering intensity changes slightly with incorporation of RF, implying that the crystalline lamellar long spacing changes very slightly with the introduction of the fiber (12.8 nm for pure PP and 13.9 nm for the composite with 30 wt % RF). Therefore, it

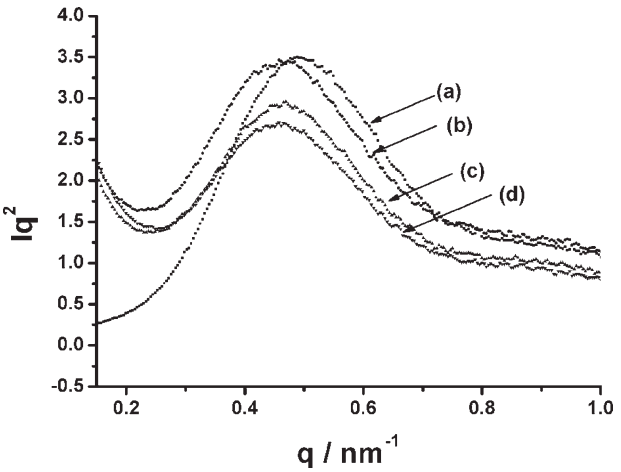

Figure 11 SAXS patterns for (a) neat PP, (b) PP/MAPP/RF (87/3/10), (c) PP/MAPP/RF (77/3/20), and (d) PP/MAPP/RF (67/3/30).

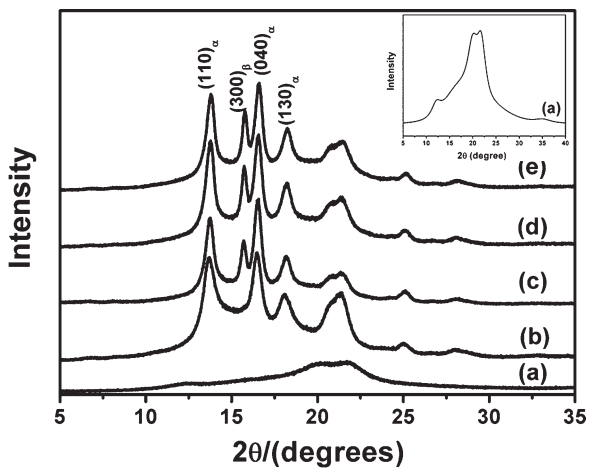

Figure 12 WAXD patterns for (a) ramie fiber, (b) neat PP, (c) PP/MAPP/RF (87/3/10), (d) PP/MAPP/RF (77/3/20), and (e) PP/MAPP/RF (67/3/30).

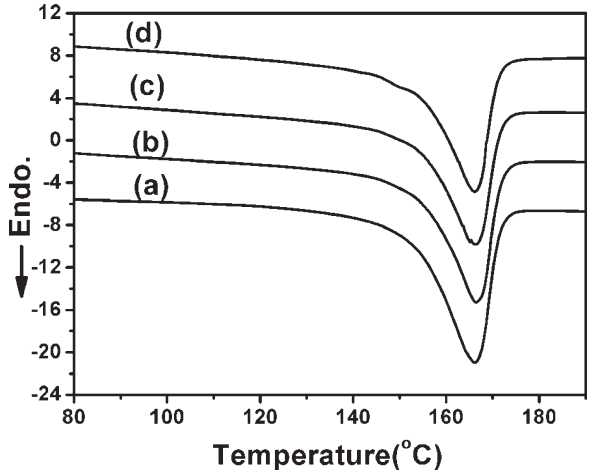

Figure 13 DSC heating curves for (a) neat PP, (b) PP/MAPP/RF (87/3/10), (c) PP/MAPP/RF (77/3/20), and (d) PP/MAPP/RF (67/3/30).

is the high aspect ratio of the fiber and good interfacial compatibility that result in the high performance of the composites.

Figure 12 shows typical wide-angle X-ray scattering patterns of the RF, pure PP, and PP/RF composites. From this figure, we can obtain the crystallinity (64%) of the fiber. Moreover, a weak peak at $2\theta = 16.0^\circ$, that is, the typical peak for the β-form PP crystals associated with (300) plane appears for the PP/RF composites, whereas it disappears for the pure PP. The result indicates that the addition of the RF induces the formation of β-form PP crystals.

Figures 13 and 14 illustrate the DSC heating and cooling thermograms for PP and PP/RF composites. The melting temperature (T_m), crystallization temperature (T_c), and heat of fusion ($\triangle H_m$) for the PP phase in these samples are listed in Table II. It is clear that the T_m briefly remains unchanged, while

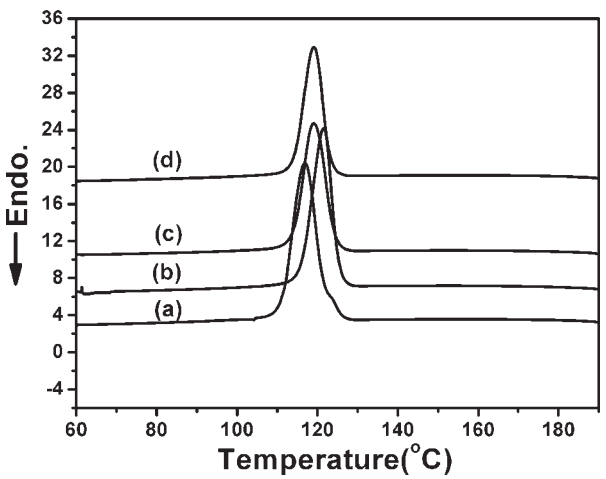

Figure 14 DSC cooling curves for (a) neat PP, (b) PP/MAPP/RF (87/3/10), (c) PP/MAPP/RF (77/3/20), and (d) PP/MAPP/RF (67/3/30).

TABLE II
Melting and Crystallization Properties of PP and the PP Phase in PP/RF Composites

Sample	T_m (°C)	T_c (°C)	ΔT (°C)	ΔH_m (J/g)	X_c (%)
PP	166.1	117.4	48.7	70.1	29.1
PP/10 wt % RF	166.4	121.7	44.7	70.5	29.3
PP/20 wt % RF	166.1	119.4	46.7	72.6	30.2
PP/30 wt % RF	166.1	119.4	46.7	82.4	34.3

the T_c increases obviously with the incorporation of the RF.

It is generally known that the degree of supercooling, $\triangle T$, which is defined as the difference between the melting temperature (T_m) and the crystallization temperature (T_c), can be used to characterize the crystallization behavior of polymer melts. A decrease in $\triangle T$ generally indicates that the crystallization rate is accelerated.[29] The $\triangle T$ values for various samples are given in Table II. It is evident that the crystallization rate of the PP phase is accelerated by the incorporation of the RF. In addition, the degree of crystallinity (X_c) for PP and PP/RF composites are also listed in Table II. It can be seen that the X_c of the PP/RF composites increases significantly with the incorporation of the RF.

CONCLUSIONS

The mechanical and thermal properties of PP can be improved by the addition of short RFs. The tensile strength and flexural strength are as high as 67 and 80 MPa by the incorporation of ramie up to 30 wt %. Therefore, the introduction of RF into PP can further extend the use of natural fiber-reinforced PP composites for semistructural or structural applications such as automotive interior parts. Morphological analysis revealed that it is the high aspect ratio of the fiber and good interfacial compatibility that result in the high performance of the composites.

References

1. Wambua, P.; Ivens, J.; Verpoest, I. Compos Sci Technol 2003, 63, 1259.
2. Fung, K. L.; Xing, X. S.; Li, R. K. Y.; Tjong, S. C.; Mai, Y. W. Compos Sci Technol 2003, 63, 1255.
3. John, M. J.; Anandjiwala, R. D. Polym Compos 2007, 29, 187.
4. Malkapuram, R.; Kumar, V.; Negi, Y. S. J Reinf Plast Compos 2009, 28, 1169.
5. Broge, J. L. Natural fibres in automotive components, Automotive Engineering International, October 2000; p120.
6. Bodros, E.; Pillin, I.; Montrelay, N.; Baley, C. Compos Sci Technol 2006, 67, 462.
7. Albuuerque, A. C.; Joseph, K.; Carvalho, L. H.; Almeida, J. R. M. Compos Sci Technol 2000, 60, 833.
8. Bledzki, A. K.; Gassan, J. Prog Polym Sci 1999, 24, 221.
9. Joseph, P. V.; Joseph, K.; Thomas, S. Compos Sci Technol 1999, 59, 1625.

10. Bos, H. L.; Müssig, J.; van den Oever, M. J. A. Compos A 2006, 37, 1591.
11. Angelov, I.; Wiedmer, S.; Evstatiev, M.; Friedrich, K.; Mennig, G. Compos A 2007, 38, 1431.
12. Panthapulakkkal, S.; Sain, M. M. J Appl Polym Sci 2007, 103, 2432.
13. Pracella, M.; Chionna, D.; Anguillesi, I.; Kulinski, Z.; Piorkowska, E. Compos Sci Technol 2006, 66, 2218.
14. van den Oever, M. J. A.; Snijder, M. H. B. J Appl Polym Sci 2008, 110, 1009.
15. Karmaker, A. C.; Youngquist, J. A. J Appl Polym Sci 1996, 62, 1147.
16. Oksman, K.; Mathew, A. P.; Langstrom, R.; Nystrom, B.; Joseph, K. Compos Sci Technol 2009, 69, 1847.
17. Zampaloni, M.; Pourboghrat, F.; Yankovich, S. A.; Rodgers, B. N.; Moore, J.; Drzal, L. T.; Mohanty, A. K.; Misra, M. Compos A 2007, 38, 1569.
18. Kim, H. S.; Lee, B. H.; Choi, S. W.; Kim, S.; Kim, H. K. Compos A 2007, 38, 1473.
19. Keener, T. J.; Stuart, R. K.; Brown, T. K. Compos A 2004, 35, 357.
20. Kumar, R.; Zhang, L. N. Compos Sci Technol 2009, 69, 555.
21. Kim, J. T.; Netravali, A. N. J Agric Food Chem 2010, 58, 5400.
22. Yu, T.; Ren, J.; Li, S. M.; Yuan, H.; Li, Y. Compos A 2010, 41, 499.
23. Krevelen, D. W. Properties of Polymers, 3rd ed. Elsevier Scientific: Amsterdam, 1997.
24. Xie, X. L.; Fung, K. L.; Li, R. K. Y.; Tjong, S. C.; Mai, Y. W. J Polym Sci Polym Phys 2002, 40, 1214.
25. Sanadi, A.; Caulfield, D. F. Compos Interf 2000, 7, 31.
26. Tajvidi, M.; Falk, R. H.; Hermanson, J. C. J Appl Polym Sci 2006, 101, 4341.
27. Fu, S. Y.; Mai, Y. W.; Ching, E. C. Y.; Li, R. K. Y. Compos A 2002, 33, 1549.
28. Glatter, O.; Kratky, O. Small-Angle X-ray Scattering. Academic Press: London, UK, 1982.
29. Xie, X. L.; Li, R. K. Y.; Tjong, S. C.; Mai, Y. W. Polym Compos 2002, 23, 319.